Two-dimensional magnetic boron

Xiang-Feng Zhou,[1,2,*] Artem R. Oganov,[2,3,4] Zhenhai Wang,[2,5] Ivan A. Popov,[6] Alexander I. Boldyrev,[6] and Hui-Tian Wang[1,7]

[1]*School of Physics and Key Laboratory of Weak-Light Nonlinear Photonics, Nankai University, Tianjin 300071, China*

[2]*Department of Geosciences, Center for Materials by Design, and Institute for Advanced Computational Science, Stony Brook University, Stony Brook, New York 11794, USA*

[3]*Skolkovo Institute of Science and Technology, 3 Nobel St., Moscow 143026, Russia*

[4]*School of Materials Science, Northwestern Polytechnical University, Xi'an 710072, China*

[5]*Peter Grünberg Research Center, Nanjing University of Posts and Telecommunications, Nanjing, Jiangsu 210003, China*

[6]*Department of Chemistry and Biochemistry, Utah State University, Logan, Utah 84322, USA*

[7]*National Laboratory of Solid State Microstructures and Collaborative Innovation Center of Advanced Microstructures, Nanjing University, Nanjing 210093, China*

We predict a two-dimensional (2D) antiferromagnetic (AFM) boron (designated as M-boron) by using *ab initio* evolutionary methodology. M-boron is entirely composed of B_{20} clusters in a hexagonal arrangement. Most strikingly, the highest valence band of M-boron is isolated, strongly localized, and quite flat, which induces spin polarization on either cap of the B_{20} cluster. This flat band originates from the unpaired electrons of the capping atoms and is responsible for magnetism. M-boron is thermodynamically metastable and is the first magnetic 2D form of elemental boron.

I. INTRODUCTION

Boron, a nearest neighbor of carbon in the Periodic Table, is an element of unique chemical and structural complexity. Its electron-deficient bonding leads to rich diversity of its crystal structures [1,2]. Boron is in many ways an analog of carbon; its nanostructures—clusters, fullerenes, nanotubes, and 2D structures—have attracted enormous attention [3–18] in the hopes of discovering unique properties, surpassing carbon. Recent prediction of the B_{80} buckyball has aroused extensive interest because of structural similarity to the C_{60} fullerene [5,19]. It was followed immediately by the proposal of stable 2D boron sheets with triangular and hexagonal motifs (named as α sheet) [6], which can serve as a building block (or precursor) for fullerenes, nanotubes, and nanoribbons. However, subsequently, buckled bilayer structures were predicted to be much more stable. Some of them turned out to have novel electronic properties, such as distorted Dirac cones [16]. For carbon, magnetism was reported in the highly oriented pyrolitic graphite with vacancies [20,21], graphite ribbons under electric field [22], tetrakis(dimethylamino)ethylene fullerene, and so on [23]. Unlike carbon, elemental boron has not been frequently reported to possess magnetism [24], much less for 2D boron even though it is a graphene analog [25]. The major reasons for the nonexistence of magnetism in 2D boron are as follows: (i) Structural complexity of boron allotropes precludes detailed theoretical optimizations of both atomic and magnetic structure, and (ii) attempts of experimental synthesis are scarce, partly due to high cost and toxicity of typically used precursors (e.g., diborane). Fortunately, a breakthrough was just made that boron sheets can be grown on the Ag (111) surface under pristine ultrahigh vacuum conditions or on copper foils by using chemical vapor deposition (CVD) [26–29]. To resolve the crystal structures of several samples

[26], we focused on some low-energy 2D structures with hexagonal or rectangular symmetry, which should match the lattice of Ag (111) substrate very well. This resulted in a serendipitous discovery of M-boron.

II. METHOD

To find the best candidate structures for experimental results, evolutionary structure searches with two alternative methods could achieve this aim. One is to build a substrate varying the number and positions of boron adatoms, and the other is to search for lowest-energy 2D-boron structures without a substrate. For the latter method, the energies and lattice parameters for the candidates should be carefully checked in order to match the lattice of substrate. Here, the latter approach was adopted for reasons of efficiency. Therefore, by using the USPEX code [30–32], evolutionary structure searches were conducted with 18, 20, 22, 24, 26, and 28 atoms per unit cell. The prime intention is to search for some thermodynamically favored, thickness-depended 2D boron structures. To include some special 2D structures, which contain B_{12} icosahedra (its thickness is ~3.7 Å) [17], the initial thickness of 2D boron structures was set to 4 Å and allowed to change during relaxation. There are many low-energy structures found by USPEX; only one particular structure was presented for discussion. The final structure relaxations used the all-electron projector-augmented wave method as implemented in the Vienna *ab initio* simulation package (VASP) [33,34]. The exchange-correlation energy was computed within the generalized gradient approximation (GGA) with the functional of Perdew, Burke, and Ernzerhof (PBE) [35]. The plane-wave cutoff energy of 600 eV and the uniform Γ-centered k-points grids with a resolution of $2\pi \times 0.04$ Å^{-1} were used. In addition, the hybrid PBE0 functional was also employed to confirm the energetic stability of several 2D boron structures [36]. Phonon dispersion curves

---
*xfzhou@nankai.edu.cn; zxf888@163.com

were computed using the PHONOPY package with the $3 \times 3 \times 1$ supercell for nonmagnetic (NM), ferromagnetic (FM), and antiferromagnetic (AFM) M-boron [37]. Spin-polarized density functional theory calculations were adopted for investigations of magnetism. For the adaptive natural density partitioning (AdNDP) chemical bonding analysis we chose an appreciably large fragment consisting of seven B_{20} fragments [38], which *a priori* should contain all the bonding elements of the whole 2D system due to its high symmetry and appropriate size. PBE0/6-31G level of theory was used. It was previously shown that AdNDP is not sensitive to the level of theory or the basis set [39]. All the AdNDP calculations were performed using the Gaussian 09 software package [40]. Molecular visualization was performed using Molekel 5.4.0.8 [41].

III. RESULTS AND DISCUSSION

The most stable structures from separate structural searches are designated from 2D-B_{18}, 2D-B_{20},..., 2D-B_{28}. As shown in Fig. 1(a), the GGA-PBE (PBE0) results yield the total energies for 2D-B_{18}, 2D-B_{20}, 2D-B_{22}, 2D-B_{24}, 2D-B_{26}, and 2D-B_{28} are -6.338 (-7.698), -6.378 (-7.756), -6.408 (-7.788), -6.364 (-7.710), $-6.432(-7.81)$, and -6.41

TABLE I. Lattice constants, atomic positions, and total energies (E_{tot}) of M-boron with NM, FM, and AFM states.

Phase	a (Å)	b (Å)	c (Å)	Atomic positions	E_{tot} (eV/atom)
NM	5.178	5.178	16.581	B_1 (0.0, 0.0, 0.366)	-6.312
				B_2 (0.668, 0.0, 0.596)	
				B_3 (0.793, 0.586, 0.5)	
FM	5.194	5.194	16.451	B_1 (0.0, 0.0, 0.365)	-6.321
				B_2 (0.666, 0.0, 0.596)	
				B_3 (0.792, 0.584, 0.5)	
AFM	5.189	5.189	16.534	B_1 (0.0, 0.0, 0.363)	-6.326
				B_2 (0.667, 0.0, 0.595)	
				B_3 (0.793, 0.586, 0.5)	
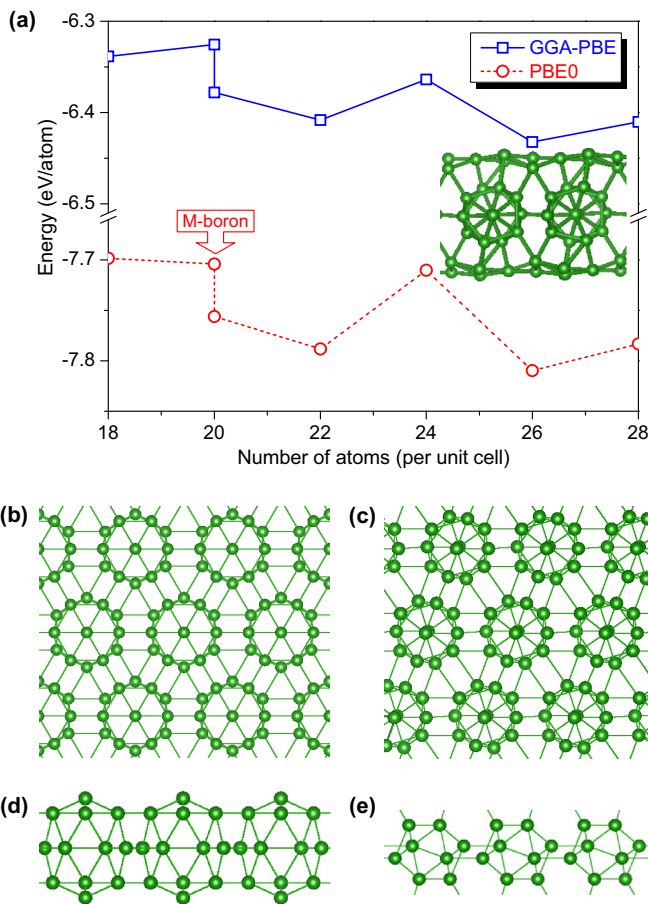
(-7.783) eV/atom, respectively. Therefore, GGA-PBE and PBE0 give the same ranking of structures by energetic stability. The inset of Fig. 1(a) shows the structure of 2D-B_{26}, where the icosahedral B_{12} units are covered by two monolayer sheets (top and down). 2D-B_{26} has the lowest energy among all of investigated 2D boron allotropes. Its $P\bar{1}$ symmetry and complex structure indicate that boron is a frustrated system [16]. The electronic structure calculations show that 2D-B_{22} and 2D-B_{28} are semiconductors with the GGA-PBE band gap of 0.45 and 0.51 eV. In contrast, other stable 2D boron forms are metals. The GGA-PBE and PBE0 results for M-boron are -6.326 and -7.704 eV/atom. This means that M-boron is a metastable phase. The crystal structures of M-boron and bulk α-boron are shown in Figs. 1(b)–1(e) [42]. The (001) projection of M-boron [Fig. 1(b)] shows dodecagonal patterns, which look very similar to those of the (111) plane of α-boron [Fig. 1(c)]. The difference is that the latter forms decagonal motif. M-boron is completely made of B_{20} cages, in contrast to the well-known B_{12} icosahedra in α-boron [Figs. 1(d) and 1(e)] and all known bulk boron allotropes. B_{20} cluster has three layers: The first and third layers are composed of hexagonal pyramids with mirror symmetry, separated by the second flat layer. Table I lists lattice constants, atomic positions, and total energies of NM, FM, and AFM states of M-boron. It shows that the AFM ordering is the ground state of M-boron, which has almost the same energy (-6.33 eV/atom) as the recently predicted 2D Dirac boron, and is lower in energy than α sheet (-6.28 eV/atom) [16]. Because there is only one B_{20} cluster per unit cell of M-boron, to confirm its magnetic surface state, we had to build a $2 \times 2 \times 1$ supercell with FM and AFM orderings for the surface, respectively. The calculations show that the FM surface state (-126.513 eV/cell) is more stable than the AFM surface state (-126.509 eV/cell). This indicates that M-boron is a 2D AFM material associated with the FM surface state.

NM M-boron is metallic with a flat band (the highest valence band) at the Fermi level, and the Fermi level crosses both the lowest conduction band and the flat band around the M point, leading to large density of states (DOS) at the Fermi level [Figs. 2(a) and 2(b)]. To stabilize the material, the high DOS at the Fermi level can be lowered either by structural (Peierls) distortion or by spin polarization [43]. Since the crystal structure of M-boron is highly symmetric

FIG. 1. (a) Total energies from the GGA-PBE and PBE0 calculations for several 2D boron structures. The inset shows the structure of 2D-B_{26}. (b) and (d) projection of M-boron structure along the [001] and [100] directions. (c) and (e) projection of α-boron along the [111] and [11$\bar{2}$] directions.
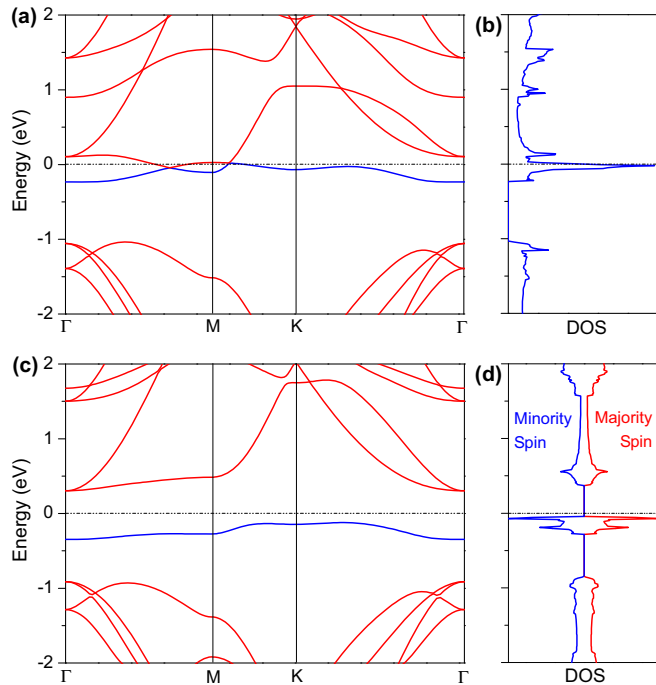
FIG. 2. Electronic properties of M-boron. (a) Band structure of NM M-boron. The Fermi level is set to zero. Most of the flat band is colored in blue; part of it is colored in red within the band crossing near the M point, (b) density of states (DOS) of NM M-boron, (c) band structure of AFM M-boron. The highest valence band (flat band) is colored in blue, (d) DOS of AFM M-boron. The majority spin is colored in red, and blue for the minority spin.

FIG. 3. Band-decomposed spin charge density and electron localization function (ELF) of AFM M-boron: (a) and (c) projection of the flat band decomposed majority-spin charge density (colored in red) along the [001] and the minority-spin charge density (colored in blue) along the [100] directions; (b) and (d) projection of the ELF in M-boron along the [001] and [100] directions. The unpaired electrons are labeled as number 1 in (b) and (d).

and strong B-B bonds make distortions difficult, the flat band may induce spin polarization of M-boron according to the Fermi level instability. The band structure and DOS of AFM M-boron are shown in Figs. 2(c) and 2(d). Due to spin polarization, the flat band is separated away from the highly dispersive conduction band, resulting in a NM-AFM transition and opening of a band gap; M-boron is an AFM semiconductor with the GGA-PBE indirect band gap of 0.43 eV [Fig. 2(c)]. Actually, as mentioned above, for M-boron we see order of stability NM < FM < AFM, which is in good agreement with the electronic stability among different states of M-boron (NM metal < FM metal [44] (Fig. S1) < AFM semiconductor). Most importantly, the isolated flat band with a dispersion of 0.23 eV [Fig. 2(c)] may play a decisive role in the emergence of magnetism. To explore the physical origin of the flat band, the band decomposed spin-polarized charge density at all k points is plotted in Figs. 3(a) and 3(c). Large bubbles of spin density are localized on top of B_1 atoms (the polar sites of the hexagonal pyramids). These bubbles represent the majority (colored in red) and minority (colored in blue) spin electrons and have the same size and shape due to mirror symmetry. The opposite spin densities above and below the plane show that M-boron is an AFM semiconductor associated with the FM surface state. The charge density distribution for the flat band is predominantly derived from the out-of-plane (p_z orbitals) states of B_1 atoms. This implies that the strongly localized flat band, mostly originating from the p_z orbitals of the B_1 atoms, is responsible for magnetism of the M-boron.

The B_{12} cluster in α-boron has 36 valence electrons, 26 of which may be used for intraicosahedral bonds and 10 for intericosahedral bonds. Each icosahedron forms six two-center-two-electron ($2c$-$2e$) bonds with the icosahedra of neighboring layers, which requires $6 \times 2/2 = 6$ electrons, as well as six closed three-center-two-electron ($3c$-$2e$) bonds with the neighboring icosahedra in its own layer, these multicenter bonds require $6 \times 2/3 = 4$ electrons. Therefore, the electrons are balanced for α-boron according to Wade's rule [1]. Since M-boron is also a semiconductor and made entirely of B_{20} clusters, it is natural to investigate the relationship between bonding and semiconducting nature of this phase. As listed in Table I, there are three inequivalent atomic positions (B_1, B_2 and B_3). For the AdNDP chemical bonding analysis, an appreciably large fragment consisting of seven B_{20} fragments was chosen, which *a priori* should contain all the bonding elements of the whole 2D system due to its high symmetry and appropriate size [Fig. 4(a)]. Since M-boron is found to be AFM in its ground state, we intentionally quenched all fourteen B_1 atoms with H atoms to deal with a single-configuration wave function. It is important to note that this inclusion does not affect a chemical bonding pattern of the 2D system, and, presumably, should result in the formation of fourteen B_1-H bonds. Next, 36 additional H atoms were added to terminate the peripheral bonding interactions of six outer B_{20} fragments with the rest of the M-boron. Clearly, the number of electrons in the proposed cluster ($B_{140}H_{50}$), which serves as a model fragment of the infinitely extended 2D M-boron, should be adjusted for the boundary conditions between the cluster being inside the extended system and its neighboring atoms, with which it shares electrons. In order to account for those shared electrons between the cluster and the neighboring atoms, the external positive charge of +34 was set. Thus, the model cluster
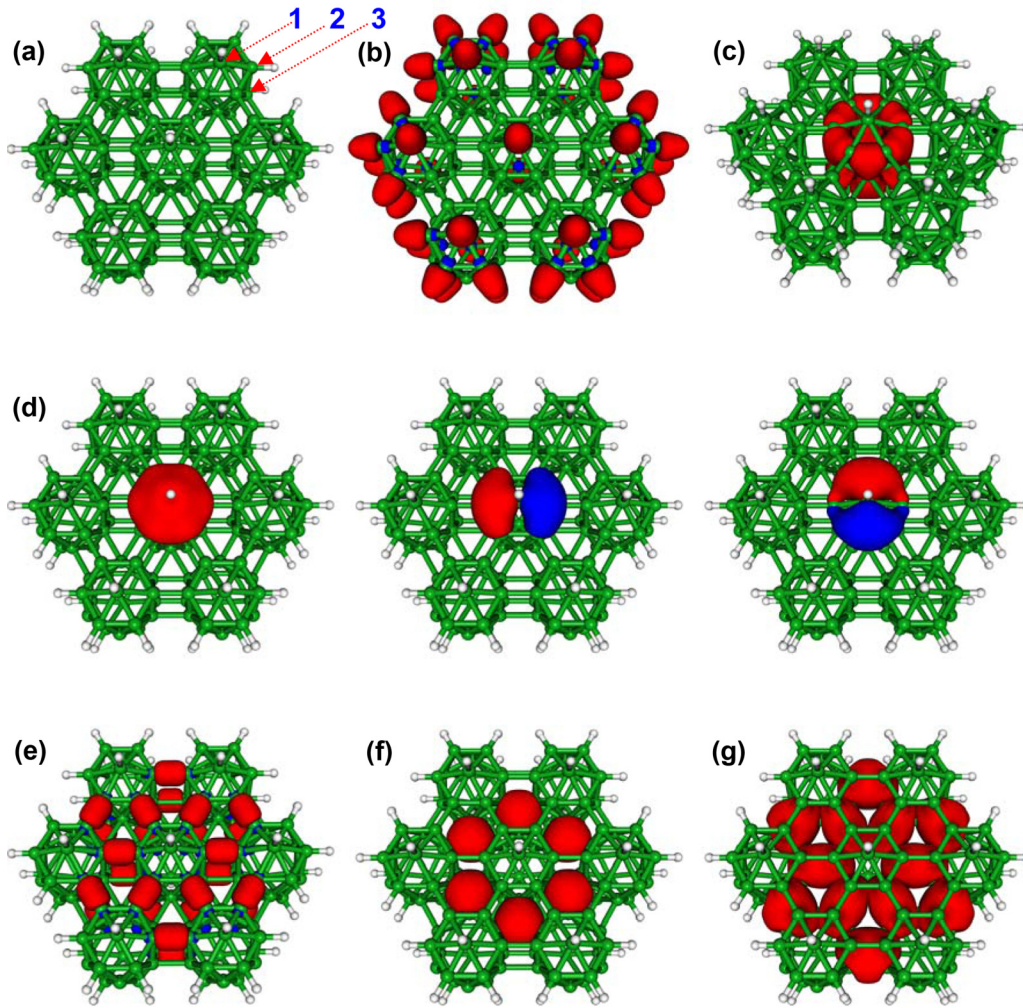
FIG. 4. Chemical bonding analysis for the model fragment of B_{20} clusters in M-boron: (a) $B_{140}H_{50}^{34+}$, where three inequivalent boron atomic positions are labeled as B_1, B_2, and B_3; (b) fifty $2c$-$2e$ B-H σ bonds with occupation numbers (ONs) in the 1.50–1.70 $|e|$ range, (c) twelve $3c$-$2e$ B_2-B_3-B_2 σ bonds with ONs = 1.82 $|e|$ forming the side frame of each B_{20} cluster, (d) three $7c$-$2e$ σ bonds with ONs = 1.84–1.93 $|e|$ found on every cap. Intercluster bonding elements: (e) twenty four classical $2c$-$2e$ B_2-B_2 σ bonds with ONs = 1.81 $|e|$ responsible for the direct bonding between B_{20} building blocks, (f) six $3c$-$2e$ B_3-B_3-B_3 σ bonds with ONs = 1.95 $|e|$ found in the middle layer, (g) twelve $8c$-$2e$ σ bonds ONs = 1.96 $|e|$ connecting all three layers of the M-boron. All the bonding elements of each type are superimposed on a single framework.

considered for the chemical bonding analysis is $B_{140}H_{50}^{34+}$. As shown in Fig. 4(b), the $2c$-$2e$ B_2-H and B_1-H σ bonds found in the $B_{140}H_{50}^{34+}$ model correspond to B_2-B_2 bonds and the lone p_z electrons on B_1 atoms in the periodic structure of the M-boron, respectively. The AdNDP chemical bonding analysis revealed two types of bonding. For intracluster bonding, there are twelve $3c$-$2e$ σ bonds [Fig. 4(c)] on the sides of each B_{20} cluster (similar to the case of all-boron fullerene [18]) and six seven-center-two-electron ($7c$-$2e$) σ bonds on two caps of the B_{20} cluster [three such bonds on each cap, as shown in Fig. 4(d)], which requires $12 \times 2 + 6 \times 2 = 36$ electrons. For intercluster bonding, there are twelve $2c$-$2e$ σ bonds [Fig. 4(e)] which connect the neighboring B_{20} clusters with B_2 atoms (at top layer), six $3c$-$2e$ σ bonds [Fig. 4(f)] which connect the B_{20} clusters with B_3 atoms (at middle layer), and six eight-center-two-electron ($8c$-$2e$) σ bonds [Fig. 4(g)] formed within all three layers of M-boron (each cluster contributes one electron). This requires $12 \times 2/2 + 6 \times 2/3 + 6 \times 1 = 22$

electrons. Occupation numbers for different kinds of bonds are close to the ideal value of two electrons, hence giving additional credibility to the chemical bonding picture of the M-boron. The most striking feature, there are two localized unpaired electrons [labeled as 1 in Figs. 3(b) and 3(d)] on the B_1 atoms are the key factors for the existence of magnetism. In total, there are $36 + 22 + 2 = 60$ electrons, which show that M-boron satisfies the electron counting rule [45,46], becoming an AFM semiconductor. For FM M-boron, the magnetic moment is 1.71 μ_B/cell. Because B_1 atoms govern magnetism, the local magnetic moment for B_1 atoms should be 0.85 μ_B (one electron per atom). Given that AFM M-boron has a FM surface state, we can reasonably infer that B_1 atoms in the AFM state may have the same local magnetic moment of 1 μ_B.

Phonon dispersion curves and phonon density of states (PDOS) show that both FM (Fig. S2a) and AFM [Figs. 5(a) and 5(b)] versions of M-boron are dynamically stable, but there are large imaginary frequencies in the NM state (Fig. S2b)

(a)

(b)

(c)
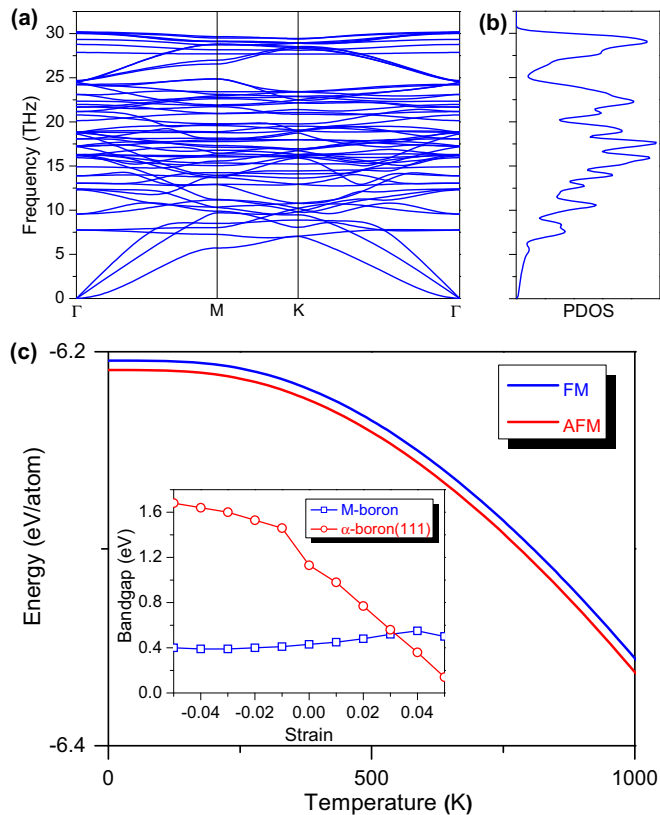
FIG. 5. Stability of M-boron. (a) Phonon dispersion curves of AFM M-boron. (b) Phonon density of states (PDOS) of M-boron. (c) Temperature dependence of the free energy for the FM and AFM states. The inset shows variation of band gap of M-boron compared with α-boron (111) surface via the biaxial tensile (negative strain) or compressive strain (positive strain).

[44]. Usually, structural phase transitions are expected to remove soft-mode instabilities. However, for M-boron, the electronic topological transition (the emergence of magnetism) is verified to be an alternative way to resolve the dynamical instability. Moreover, in order to take the zero-point energy and temperature effects into account, we computed harmonic free energy for both the FM and AFM states. The temperature dependence of the free energy for the FM and AFM M-boron is shown in Fig. 5(c). It shows that AFM M-boron is always more stable than FM M-boron up to the temperature of 1000 K. Additionally, since the electronic properties of materials can be tuned by external strain, it is of great interest to study the influence of biaxial tensile or compressive strain on the band gap of AFM M-boron with respect to the reconstructed α-boron (111) surface [Fig. 5(c)] [17]. The band gap of the α-boron (111) surface increases or decreases with biaxial tensile or compressive strain, respectively. The semiconducting α-boron (111) surface shows a normal strain

behavior just like the compression behavior of α-boron under pressure [2]. In contrast, the band gap of M-boron is almost insensitive to strains of up to 5% (when compressive strain exceeds 6%, an AFM-NM transition takes place because further increasing compressive strain strengthens interactions among the unpaired electrons, which eventually destroy its AFM state). The position and width of the flat band are almost fixed and independent of tensile or compressive strain, guaranteeing robustness of magnetism. M-boron can endure large strain, persisting in its AFM state. Therefore, it is practicable to grow M-boron on some metal surfaces and expect it to be magnetic, because the lattice mismatch is less than 4% for Ag (111), 2% for Cu (111). Recently, boron thin films were prepared on Cu substrate by CVD technology and shown to be slices of the γ-B_{28} structure, just a few atoms thick. This suggests that synthesis of M-boron is also possible in similar conditions [27].

IV. CONCLUSION

In summary, we have predicted 2D magnetic boron by using an *ab initio* evolutionary structure search combined with spin-resolved electronic structure calculations. M-boron is thermodynamically metastable with rare AFM state, which bridges the gap between boron clusters and 2D nanomaterials and opens a path to explore light elemental magnetic materials at atomic scale.

[1] B. Albert and H. Hillebrecht, Angew. Chem. Int. Ed. **48**, 8640 (2009).

[2] A. R. Oganov, J. H. Chen, C. Gatti, Y. Z. Ma, Y. M. Ma, C. W. Glass, Z. X. Liu, T. Yu, O. O.

Kurakevych, and V. L. Solozhenko, Nature (London) **457**, 863 (2009).

[3] H. J. Zhai, B. Kiran, J. Li, and L. S. Wang, Nat. Mater. **2**, 827 (2003).

[4] I. Boustani, Surf. Sci. **370**, 355 (1997); Phys. Rev. B **55**, 16426 (1997).

[5] N. Gonzalez Szwacki, A. Sadrzadeh, and B. I. Yakobson, Phys. Rev. Lett. **98**, 166804 (2007).

[6] H. Tang and S. Ismail-Beigi, Phys. Rev. Lett. **99**, 115501 (2007).

[7] Dasari L. V. K. Prasad and Eluvathingal D. Jemmis, Phys. Rev. Lett. **100**, 165504 (2008).

[8] H. Tang and S. Ismail-Beigi, Phys. Rev. B **80**, 134113 (2009); **82**, 115412 (2010).

[9] S. Saxena and T. A. Tyson, Phys. Rev. Lett. **104**, 245502 (2010).

[10] S. De, A. Willand, M. Amsler, P. Pochet, L. Genovese, and S. Goedecker, Phys. Rev. Lett. **106**, 225502 (2011).

[11] F. Liu, C. Shen, Z. Su, X. Ding, S. Deng, J. Chen, N. Xu, and H. Gao, J. Mater. Chem. **20**, 2197 (2010).

[12] E. S. Penev, S. Bhowmick, A. Sadrzadeh, and B. I. Yakobson, Nano Lett. **12**, 2441 (2012).

[13] X. Wu, J. Dai, Y. Zhao, Z. Zhuo, J. Yang, and X. C. Zeng, ACS Nano **6**, 7443 (2012).

[14] H. Liu, J. Gao, and J. Zhao, Sci. Rep. **3**, 3238 (2013).

[15] M. Amsler, S. Botti, Miguel A. L. Marques, and S. Goedecker, Phys. Rev. Lett. **111**, 136101 (2013).

[16] X. F. Zhou, X. Dong, A. R. Oganov, Q. Zhu, Y. Tian, and H. T. Wang, Phys. Rev. Lett. **112**, 085502 (2014).

[17] X. F. Zhou, A. R. Oganov, X. Shao, Q. Zhu, and H. T. Wang, Phys. Rev. Lett. **113**, 176101 (2014).

[18] H.-J. Zhai, Y.-F. Zhao, W.-L. Li, Q. Chen, H. Bai, H.-S. Hu, Z. A. Piazza, W.-J. Tian, H.-G. Lu, Y.-B. Wu, Y.-W. Mu, G.-F. Wei, Z.-P. Liu, J. Li, S.-D. Li, and L.-S. Wang, Nat. Chem. **6**, 727 (2014).

[19] H. W. Kroto, J. R. Heath, S. C. O'Brien, R. F. Curl, and R. E. Smalley, Nature (London) **318**, 162 (1985).

[20] P. Esquinazi, A. Setzer, R. Höhne, C. Semmelhack, Y. Kopelevich, D. Spemann, T. Butz, B. Kohlstrunk, and M. Lösche, Phys. Rev. B **66**, 024429 (2002).

[21] Y. Zhang, S. Talapatra, S. Kar, R. Vajtai, S. K. Nayak, and P. M. Ajayan, Phys. Rev. Lett. **99**, 107201 (2007).

[22] Y. W. Son, M. L. Cohen, and S. G. Louie, Nature (London) **444**, 347 (2006).

[23] B. Narymbetov, A. Omerzu, V. V. Kabanov, M. Tokumoto, H. Kobayashi, and D. Mihailovic, Nature (London) **407**, 883 (2000).

[24] S. Botti, A. Castro, N. N. Lathiotakis, X. Andrade, and Miguel A. L. Marques, Phys. Chem. Chem. Phys. **11**, 4523 (2009).

[25] K. S. Novoselov, A. K. Geim, S. V. Morozov, D. Jiang, M. I. Katsnelson, I. V. Grigorieva, S. V. Dubonos, and A. A. Firsov, Nature (London) **438**, 197 (2005).

[26] A. J. Mannix, X. F. Zhou, B. Kiraly, J. D. Wood, D. Alducin, B. D. Myers, X. Liu, B. L. Fisher, U. Santiago, J. R. Guest, M. J. Yacaman, A. Ponce, A. R. Oganov, M. C. Hersam, and N. P. Guisinger, Science **350**, 1513 (2015).

[27] G. Tai, T. Hu, Y. Zhou, X. Wang, J. Kong, T. Zeng, Y. You, and Q. Wang, Angew. Chem. Int. Ed. **54**, 15473 (2015).

[28] B. Feng, J. Zhang, Q. Zhong, W. Li, S. Li, H. Li, P. Cheng, S. Meng, L. Chen, and K. Wu, arXiv:1512.05029.

[29] B. Feng, J. Zhang, R. Y. Liu, I. Takushi, C. Lian, L. Chen, K. Wu, H. Li, S. Meng, F. Komori, and I. Matsuda, arXiv:1512.05270.

[30] A. R. Oganov and C. W. Glass, J. Chem. Phys. **124**, 244704 (2006).

[31] A. R. Oganov, A. O. Lyakhov, and M. Valle, Acc. Chem. Res. **44**, 227 (2011).

[32] A. O. Lyakhov, A. R. Oganov, H. T. Stokes, and Q. Zhu, Comput. Phys. Commun. **184**, 1172 (2013).

[33] P. E. Blöchl, Phys. Rev. B **50**, 17953 (1994).

[34] G. Kresse and J. Furthmüller, Phys. Rev. B **54**, 11169 (1996); Comput. Mater. Sci. **6**, 15 (1996).

[35] J. P. Perdew, K. Burke, and M. Ernzerhof, Phys. Rev. Lett. **77**, 3865 (1996).

[36] J. Paier, R. Hirschl, M. Marsman, and G. Kresse, J. Chem. Phys. **122**, 234102 (2005).

[37] A. Togo, F. Oba, and I. Tanaka, Phys. Rev. B **78**, 134106 (2008).

[38] D. Y. Zubarev and A. I. Boldyrev, Phys. Chem. Chem. Phys. **10**, 5207 (2008).

[39] A. P. Sergeeva and A. I. Boldyrev, Comments Inorg. Chem. **31**, 2 (2010).

[40] M. J. Frisch *et al.*, *GAUSSIAN09, Revision B.01*, Gaussian, Inc, Wallingford, CT, 2009.

[41] U. Varetto, *MOLEKEL 5.4.0.8*, Swiss National Supercomputing Centre, Manno Switzerland, 2009.

[42] B. F. Decker and J. S. Kasper, Acta Crystallogr. **12**, 503 (1959).

[43] Y. Liang, X. Yuan, Y. Gao, W. Zhang, and P. Zhang, Phys. Rev. Lett. **113**, 176401 (2014).

[44] See Supplemental Material at http://link.aps.org/supplemental/10.1103/PhysRevB.93.085406 for the additional results of *M*-boron and the structural parameters of other stable 2D boron sheets.

[45] C. B. Duke, Chem. Rev. **96**, 1237 (1996).

[46] M. D. Pashley, Phys. Rev. B **40**, 10481 (1989).